Bull. Mater. Sci., Vol. 40, No. 1, February 2017, pp. 195–199. © Indian Academy of Sciences.
DOI 10.1007/s12034-016-1340-6

Sub-micron-sized delafossite $CuCrO_2$ with different morphologies synthesized by nitrate–citric acid sol–gel route

SATISH BOLLOJU[1] and RADHAKRISHNAN SRINIVASAN[1,2,*]
[1]Department of Chemistry, BITS Pilani, Hyderabad Campus, Hyderabad 500 078, India
[2]Present address: Department of Chemistry, BMS Institute of Technology, Bangalore 560064, India

MS received 31 August 2015; accepted 25 May 2016

Abstract. **Currently, copper chromium oxide crystallizing in delafossite structure attracts huge research interest due to its versatile applications arising from its layered structure. In this work, delafossite $CuCrO_2$ was synthesized by sol–gel method from their respective hydrated nitrate salts with citric acid as a chelating agent. The phase formation temperature was found to be between 750 and 775°C. At 750°C, the partial formation of delafossite $CuCrO_2$ spheres with particle size in nano-regime was observed in the midst of platelets of spinel $CuCr_2O_4$. A green coloured powder with particle size 125–350 nm exhibiting distorted spheres was obtained at 775°C. The increase in temperature has a profound impact on the particle size, morphology and the optical properties of $CuCrO_2$. The X-ray powder diffraction studies revealed the formation of 3R-$CuCrO_2$ phase (rhombohedral, space group R-3m) as a major product in the temperature range 775–1000°C. The unit cell parameters were found to be $a = b = 2.9711$ Å and $c = 17.0723$ Å at 1000°C. Scanning electron micrographs illustrated the different morphologies from spheres to hexagonal form via distorted spheres and cubes. The UV–Vis diffuse reflectance spectra measured for the powders exhibited semiconductor characteristics with an interesting size-related and temperature-dependent bandgap.**

Keywords. **Delafossite; semiconductors; sol–gel; morphology; particle size.**

1. Introduction

Delafossite oxides of form ABO_2, where A = Cu, Ag and B = Al, Ga, In, Cr, La, Y, B, etc., are attracting huge research interest in recent years due to their potential application as p-type transparent conducting oxides, thermoelectric material, catalyst, photocatalyst, sensors and p-type transparent electrodes for dye-sensitized solar cells [1–7]. The layered structure of $CuCrO_2$ contains natural superlattices consisting of alternate layers of edge-shared CrO_6 octahedral and dumbbell-shaped CuO_2 units. Delafossite $CuCrO_2$ is synthesized by solid-state [8–10], hydrothermal [11–13], self-combustion [14] and sol–gel [15] routes. Also, a microwave-assisted synthesis of delafossite $CuCrO_2$ was reported [16].

Delafossite $CuCrO_2$ is an important system and a number of publications report the theoretical and experimental work on its p-type conductivity, magnetism and transport properties [17–19]. Compared with n type, p-type TCOs are relatively rare but have gained momentum in research over the last decade after the discovery of p-type conductivity in $CuAlO_2$ thin films by Kawazoe *et al* [20]. So far, from the literature, the lowest resistivity in p-type TCO was found to be in Mg-doped $CuCrO_2$ films [21]. However, in comparison with thin films, reports on nano- or sub-micron powder are scarce and it is important to understand their phase formation temperature or other mentioned property studies. A direct bandgap was reported to be fundamental for thin films and an indirect gap was found to be fundamental in some of the reported work [22–27].

Soft-chemistry routes like hydrothermal and sol–gel are used in particular to synthesize delafossite $CuCrO_2$ nanopowders. Hydrothermal/solvothermal syntheses of copper and silver delafossite oxides leading to micron, sub-micron and nano-sized powders are comparatively well studied by different groups [28–31]. Sol–gel synthesis in general has advantages with respect to obtaining the metastable materials with purity and compositional homogeneity at moderate temperatures in comparison with the high-temperature ceramic route. Also, the particle morphologies are influenced by the presence of chelating agents during the chemical transformation of the molecular precursor to the final oxide [5,32]. In this article, sol–gel synthesis of $CuCrO_2$ with particle size ranging from sub-micron to several microns at different temperatures along with their morphological and optical changes are reported with the aid of powder X-ray diffraction (PXRD), SEM, UV–Vis diffuse reflectance spectra and FT-IR spectra.

*Author for correspondence (srinivasan.r@bmsit.in, rsvasan31@gmail.com)

2. Experimental

2.1 *Synthesis*

$Cu(NO_3)_2{\cdot}3H_2O$ (from SDFCL) and $Cr(NO_3)_3{\cdot}9H_2O$ (from NR CHEM) in a 1:1 molar ratio were dissolved in distilled water and properly mixed by constant stirring. Two equivalents of citric acid (extrapure, from SDFCL) were added into it while stirring. The ratio of the metal ions to citric acid was one [33]. The obtained green coloured solution was treated at 100°C to evaporate the water content. On complete evaporation of water, a green transparent gel was formed. Subsequently, the gel was dried in a hot air oven to obtain a black foamy powder. This black powder was used as a precursor for calcination at different temperatures. Typically, the precursor was placed in a recrystallized alumina crucible and slowly heated to the required temperature at the rate of 5°C min^{-1}. Then the crucible was allowed to dwell for the required duration before cooling it to reach the room temperature [34]. In this work, unless and otherwise stated, the precursors were calcined for 4-h duration at different temperatures for explaining the results with respect to phase analysis, particle size and optical properties. The obtained delafossite $CuCrO_2$ powders were washed with liquid ammonia followed by dilute HNO_3 and distilled water to remove the CuO impurities.

2.2 *PXRD studies*

PXRD data were collected in a PANalytical XPERT-PRO Diffractometer ($\lambda = 1.54060$ Å) operating at 40 kV and 30 MA. By scanning every 0.05° for 10.16 s, data were collected for the two theta range of 10–80°. Powder cell software was used to generate the theoretical powder pattern from the literature. The unit cell parameters were obtained using the Unit cell software.

2.3 *SEM analysis*

SEM measurements were carried out by a JEOL JSM-840A.

2.4 *UV–vis diffuse reflectance studies*

The washed powders of delafossite $CuCrO_2$ were used for UV–Vis diffuse reflectance studies. Data were collected over the spectral range 200–870 nm using a JASCO V-750 UV–Vis spectrometer equipped with an integrating sphere (60 mm diameter, ISV-722 attachment). Background spectra for baseline correction were obtained using the supplied standard white plate. Data were collected with a scan speed of 200 nm min^{-1}, data interval of 1 nm and a signal bandwidth of 5 nm. The reflectance data were transformed into an absorption data (α/s) by using the Kubelka and Munk equation, $\alpha/s = (1-R)^2/2R$, where α is the absorption coefficient, s the scattering coefficient and R the diffuse reflectance.

2.5 *FT-IR spectra*

Spectra were recorded with a JASCO FT-IR spectrometer using KBr pellets between 400 and 4000 cm^{-1}.

3. Results and discussion

Thermal analysis for the black precursor showed a complete decomposition around 350°C, which corresponds to the dehydration of water and decomposition of organic part. Information regarding the formation temperature of spinel and delafossite phases were not clear. Hence the calcinations of precursor were performed at different temperature ranging from 350 to 1000°C for different durations from 2 to 8 h in order to understand the phase formation temperature. The possible role of citric acid in this synthesis is to chelate with the metal ions in order to prevent it from precipitation as hydroxylated species and it increases the solubility to form a stable sol. Also, the nitrate–citrate route is a low-temperature redox-type exothermic reaction that provides milder reaction condition than the solid-state method [5,35]. Spinel $CuCr_2O_4$ along with CuO was formed at 600°C for 8-h duration. As already noted in the synthesis part, the following results and discussions are for the precursor calcined to 4-h duration. At 750°C, there was a clear formation of delafossite $CuCrO_2$ as a minor phase along with spinel $CuCr_2O_4$ and CuO as the major phases. At 775°C, spinel phase was converted to delafossite phase with traces of spinel and CuO as a side phase. PXRD patterns of the powders obtained at 775, 800, 900 and 1000°C are shown in figure 1 along with the theoretical pattern. The (*hkl*) values generated from the powder cell are indicated in the theoretical pattern. As shown in the figure 1, delafossite $CuCrO_2$ formed was crystalline in nature and the reflections are in agreement with the 3R-$CuCrO_2$ phase (rhombhohedral, spacegroup: R-3m (166); JCPDS Card No. 89-0539). The phases present at each temperature are given in table 1. At 1000°C, phase-pure delafossite was formed without any side phases as an impurity. The unit cell parameters obtained for the powders are mentioned in table 2.

In comparison to the solid-state synthesis route, the phase formation of spinel was at the same temperature of 600°C, but delafossite phase formation was at a lower temperature of 750–775°C with particle size in nano-size regime. FT-IR spectra of $CuCrO_2$ powders obtained at 725–800°C are shown in figure 2 and the characteristic peaks were found in the region below 1000 cm^{-1} and hence only the regions from 1200 to 400 cm^{-1} are considered. The peaks obtained around 550 and 725 cm^{-1} were assigned to the CrO_6 octohedral modes of delafossite phase in accord with the literature [29,36]. It is very clear that the IR spectra are different for powders at 725 and 750°C in comparison with 775 and 800°C and thus exemplify the phase formation temperature of delafossite phase.

The formation of spheres at 750°C with particle size around 100–125 nm is shown in the SEM micrograph

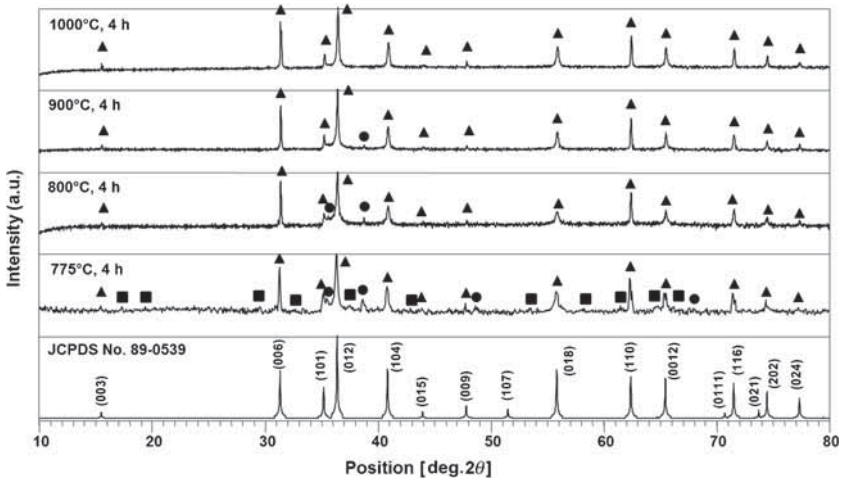

Figure 1. X-ray powder diffraction pattern of the obtained $CuCrO_2$ powders (▲: $CuCrO_2$, ■: $CuCr_2O_4$, ●: CuO).

Table 1. Summary of the results obtained for delafossite $CuCrO_2$.

Reaction temperature (°C)	Phases formed	Morphology of $CuCrO_2$	Particle size range	Colour
750	$CuCrO_2$ (minor), $CuCr_2O_4$ (major), CuO	Spheres	100–125 nm	Black
775	$CuCrO_2$, $CuCr_2O_4$ (traces), CuO	Distorted spheres	120–350 nm	Dark green
800	$CuCrO_2$, CuO	Cubes	200–500 nm	Green
900	$CuCrO_2$, CuO	Distorted cubes	500–800 nm	Green
1000	$CuCrO_2$	Distorted hexagonal	1–3 microns	Black

Table 2. Unit cell parameters of delafossite 3R-$CuCrO_2$ phase (rhombhohedral, spacegroup: R-3m).

Reaction temperature (°C)	*a* (Å)	*c* (Å)
775	2.9772	17.1322
800	2.9728	17.0803
900	2.9724	17.0795
1000	2.9711	17.0723

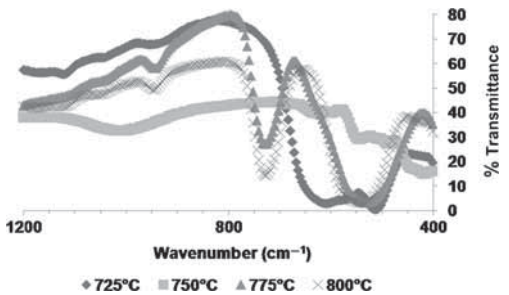

Figure 2. FT-IR spectra of obtained $CuCrO_2$ powders.

(figure 3a and b). The spheres grew in size to form a distorted sphere of particle size around 120–350 nm at 775°C for 4-h duration (figure 3c). Further evolution of morphology into cubes and distorted cubes (figure 3d and e) at 800 and 900°C, respectively, are illustrated in the SEM micrographs. The phases present are tabulated in table 1 according to the PXRD studies whereas the morphology and particle sizes are based on the SEM studies. The colours of the obtained $CuCrO_2$ powders were green till 950°C and then turned black. UV–Vis diffuse reflectance spectra measured at 800–1000°C are shown in figure 4. In figure 4, the Kubelka–Munk transformed absorption (α/s) was plotted *vs*. eV and the bandgap was then determined using a standard method in which the absorption edges were extrapolated to zero [11].

An interesting temperature as well as a size-related bandgap dependence is observed from figure 4. At 800°C, there are transitions absorbed at around 2.7, 2.3 and 1.7 eV. The transition at 2.7 eV increases to 2.9 eV on increasing the synthesis temperature to 1000°C. Thus at 800°C, the transition at 2.7 eV corresponds to a direct allowed transion and much lower than the reported value of 2.95–3.30 eV in the literature and the transition at 2.3 eV corresponds to an indirect transition. The transitions at 1.7 eV might be due to the CuO impurity. A clear red-shift towards longer wavelength is illustrated in figure 4 with the increase of temperature. Optical absorption increases with the increase of temperature due to phonon assistance and hence there is a decrease in indirect bandgap. The energy bandgap of semiconductors tends to decrease as the temperature is increased because the interatomic spacing increases when the amplitude of the atomic vibrations increases due to the increased thermal energy [37].

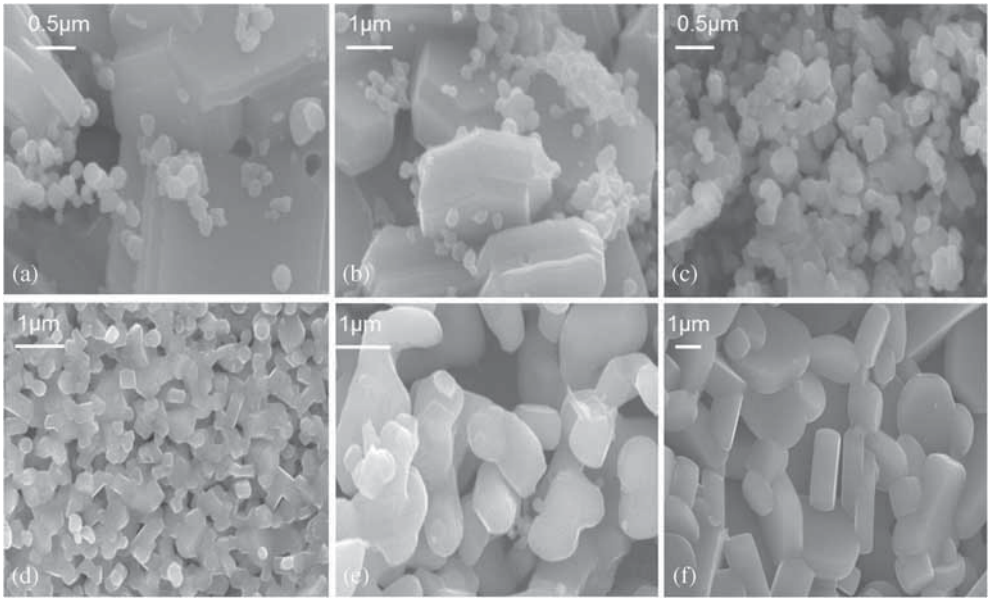

Figure 3. SEM micrographs of the obtained $CuCrO_2$ powders at (**a**, **b**) 750, (**c**) 775, (**d**) 800, (**e**) 900 and (**f**) 1000°C.

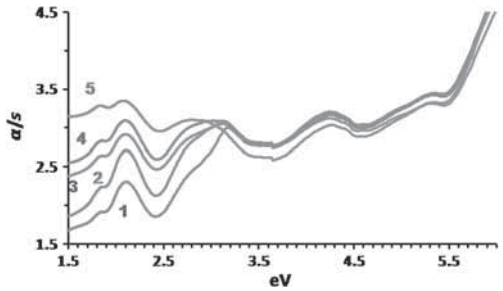

Figure 4. UV–Vis diffuse reflectance spectra of the obtained $CuCrO_2$ powders at (**1**) 800, (**2**) 850, (**3**) 900, (**4**) 950 and (**5**) 1000°C.

4. Conclusions

Sol–gel synthesis route was successfully used to synthesize sub-micron-sized delafossite $CuCrO_2$. The phase formation temperature of delafossite $CuCrO_2$ was found to be between 750 and 775°C. Particles with size ranging from about 100 nm to several microns were synthesized depending on the reaction temperature. Morphological features evolved from sphere to hexagonal via distorted spheres and cubes. UV–Vis diffuse reflectance studies indicated an interesting size- and temperature-dependent indirect bandgap. The respective direct and indirect transitions were found to be 2.7 and 2.3 eV for delafossite $CuCrO_2$ obtained at 800°C.

Acknowledgements

Department of Science and Technology (DST SERB) is acknowledged for funding through the FASTTRACK scheme (No. SR/FT/CS-024/2010). We wish to thank the Department of Physics, Alagappa University at Karaikudi, Centre for Nano Science and Technology, Karunya University at Coimbatore and University of Hyderabad for characterization facilities.

References

[1] Marquardt M A, Ashmore N A and Cann D P 2006 *Thin Solid Films* **496** 146

[2] Amrute A P, Larrazabal G O, Mondelli C and Ramirez J P 2013 *Angew. Chem. Int. Ed.* **52** 9772

[3] Zhou S, Fang X, Deng Z, Li D, Dong W, Tao R, Meng G and Wang T 2009 *Sensor Actuat. B* **143** 119

[4] Kameoka S, Okada M and Tsai A P 2008 *Catal. Lett.* **120** 252

[5] Meng Q, Lu S, Lu S and Xiang Y 2012 *J. Sol–Gel Sci. Technol.* **63** 1

[6] Powar S, Xiong D, Daeneke T, Ma M T, Gupta A, Lee G, Makuta S, Tachibana Y, Chen W, Spiccia L, Cheng Y B, Goetz G, Baeuerle P and Bach U 2014 *J. Phys. Chem. C* **118** 16375

[7] Xiong D, Zhang W, Zeng X, Xu Z, Chen W, Cui J, Wang M, Sun L and Cheng Y B 2013 *ChemSusChem* **6** 1432

[8] Shannon R D, Rogers D B and Prewitt C T 1971 *Inorg. Chem.* **10** 713

[9] Ketir W, Saadi S and Trari M 2012 *J. Solid State Eletrochem.* **16** 213

[10] Amrute A P, Lodziana Z, Mondelli C, Krumeich F and Ramirez J P 2014 *Chem. Mater.* **25** 4423

[11] Sheets W C, Mugnier E, Barnabe A, Marks T J and Poeppelmeier K R 2006 *Chem. Mater.* **18** 7

[12] Zhou S, Fang X, Deng Z, Li D, Dong W, Tao R, Meng G, Wang T and Zhu X 2008 *J. Cryst. Growth* **310** 5375

[13] Miclau M, Ursu D, Kumar S and Grozescu I 2012 *J. Nanopart. Res.* **14** 1110

[14] Chiu T W, Yu B S, Wang Y R, Chen K T and Lin Y T 2011 *J. Alloys Compd.* **509** 2933

[15] Deng Z, Zhu X, Tao R, Dong W and Fang X 2007 *Mater. Lett.* **61** 686

[16] Kumar S, Marinela S, Miclau M and Martin C 2012 *Mater. Lett.* **70** 40

[17] Okuda T, Jufuku N, Hidaka S and Terada N 2005 *Phy. Rev. B* **72** 144403(1)

[18] Poienar M, Hardy V, Kundys B, Singh K, Maignan A, Damay F and Martin C 2012 *J. Solid State Chem.* **185** 56

[19] Goetzendoerfer S, Polenzky C, Ulrich S and Loebmann P 2009 *Thin Solid Films* **518** 1153

[20] Kawazoe H, Yasukawa M, Hyodo H, Kurita M, Yanagi H and Hosono H 1997 *Nature* **389** 939

[21] Nagarajan R, Draeske A D, Sleight A W and Tate J 2001 *J. Appl. Phys.* **89** 8022

[22] Benko F A and Koffyberg F P 1986 *Mater. Res. Bull.* **21** 753

[23] Mahapatra S and Shivasankar S A 2003 *Chem. Vap. Deposition* **9** 238

[24] Li D, Fang X D, Deng Z H, Zhou S, Tao R H, Dong W W, Wang T, Zhao Y P, Meng G and Zhu X B 2007 *J. Phys. D*: *Appl. Phys.* **40** 4910

[25] Scanlon D O and Watson G W 2011 *J. Mater. Chem.* **21** 3655

[26] Bywalez R, Goetzendoerfer S and Loebmann P 2010 *J. Mater. Chem.* **20** 6562

[27] Li D, Fang X, Zhao A, Deng Z, Dong W and Tao R 2010 *Vacuum* **84** 851

[28] Xiong D, Zeng X, Zhang W, Chen W, Xu X, Wang M and Cheng Y B 2012 *J. Mater. Chem.* **22** 24760

[29] Ursu D and Miclau M 2014 *J. Nanopart. Res.* **16** 2160

[30] Srinivasan R, Chavillon B, Dossier-Brochard C, Cario L, Paris M, Gautron E, Deniard P, Odobel F and Jobic S 2008 *J. Mater. Chem.* **18** 5647

[31] Chavillon B, Cario L, Dossier-Brochard C, Srinivasan R, Le Pleux L, Pellegrin Y, Blart E, Odobel F and Jobic S 2010 *Phys. Status Solidi A* **207** 1642

[32] Goetzendoerfer S, Bywalez R and Loebmann P 2009 *J. Sol–Gel Sci. Technol.* **52** 113

[33] Ahmad A, Jagadale T, Dhas V, Khan S, Patil S, Pasricha R, Ravi V and Ogale S B 2007 *Adv. Mater.* **19** 3295

[34] Srinivasan R and Bolloju S 2014 *AIP Conf. Proc.* **1576** 205

[35] Singh K A and Pathak L C 2007 *Ceram. Int.* **33** 1463

[36] Saadi S, Bouguelia A and Trari M 2006 *Sol. Energy* **80** 272

[37] Zeghbroeck B V 2011 *Principle of semiconductor devices*, http://ecee.colorado.edu/~bart/book/book/contents.htm (University of Colorado)